CMOS INTEGRATED ORGANIC CILIARY ACTUATOR ARRAYS FOR GENERAL-PURPOSE MICROMANIPULATION TASKS

John W. Suh
R. Bruce Darling
Karl F. Böhringer
Bruce R. Donald
Henry Baltes
Gregory T. A. Kovacs

Abstract   The first micromachined bimorph organic ciliary array with on-chip CMOS circuitry is presented. This device is composed of an 8×8 array of cells each having four orthogonally oriented actuators in an overall die size of 9.4mm $\times$ 9.4mm. The polyimide based actuators were fabricated directly above the selection and drive circuitry. Selection and activation of actuators in this array shows that integration was successful.

The array was programmed to perform several kinds of manipulation tasks, including linear translation, diagonal motion, as well as vector field operations such as squeeze field and radial field orienting and centering. Preliminary experiments were also performed with the first implementation of a "universal field" that uniquely positions and orients any non-symmetric part without programming or sensor feedback. All tasks were demonstrated using thin silicon dice of about 3mm $\times$ 3mm $\times$ 0.5mm size as the object being moved.

1   INTRODUCTION

One of the potential applications of MEMS actuators is in the moving and positioning of small parts because the actuators themselves are on a similar scale (Busch-Vishniac, 1991). Toward the realization of this goal, researchers have been designing and building arrayed actuator systems that can overcome some of the inherent limitations of most microactuators (limited range of motion, degrees of freedom, and force

output) through the arrangement of actuators in series or parallel (Bobbio et al., 1991; Chen et al., 1991; Minami et al., 1993). A variety of actuation methods have been used including air jets (Pister et al., 1990; Konishi and Fujita, 1994; Mita et al., 1997), electromagnetic actuators (Liu et al., 1995; Liu and Will, 1995; Nakazawa et al., 1997), piezoelectric actuators (Furuhata et al., 1991), electrostatic actuators (Böhringer et al., 1996), and thermal bimorph actuators (Takeshima and Fujita, 1991; Ataka et al., 1993; Suh et al., 1997). Whatever the chosen actuation method, the actuators have two fundamental requirements: (1) the generation of enough force or torque to move not only themselves, but also to move external objects and (2) the generation of large displacements of the moving parts or of the media in which the parts move (e.g., air jets). The previously reported ciliary arrays (Suh et al., 1996; Suh et al., 1997) were, to our knowledge, the first ones able to move small parts in a controlled and repeatable manner along any user-chosen direction in an x-y plane.

The arrayed actuators described herein are deformable microstructures that curl into and out of the substrate plane. The curling of the actuators is due to the different coefficients of thermal expansion (CTE) of two polyimide layers that make up the structures. An integrated heater resistor is sandwiched between the two polyimide layers. When an electric current is passed through the heater resistor, the temperature of the actuator increases, and the structure (initially deflected out-of-plane) deflects downward into the plane producing both horizontal and vertical displacements. Objects that are placed on the array can be made to move by coordinating the deflections of such actuators.

Another goal of some MEMS researchers has been to merge microelectronics and micromachined transducers since the advantages gained by miniaturization and parallel fabrication can be more fully exploited by closely integrating electronic functions (Baltes, 1993; Baltes, 1996; Berlin and Gabriel, 1997). Different approaches have been taken, including carrying out bulk micromachining processes on completed dice or whole wafers (Klaassen et al., 1996; Lund and Wise, 1994; Moser et al., 1991), the interlacing of micromachining steps within a modified CMOS process (Howe, 1995; Offenberg et al., 1995), the packaging of hybrid solutions by flip-chip or wire bonding (Spangler and Kemp, 1996), the processing of MEMS features prior to CMOS processing (Nasby et al., 1996), and the post-processing of standard CMOS to add surface micromachined transducers (Hornbeck, 1995; French, 1996). For an early discussion of circuit integration as applied to distributed actuator arrays see (Fujita and Gabriel, 1991).

The purpose of this paper is to describe the first functional ciliary actuator array integrated with CMOS circuitry, providing a means for activating individual cilia and enabling the functions of the array to be altered by software. The overall architecture of the chip and major features are discussed in Section 2. The microfabrication process used to create this ciliary actuator array is described in a separate paper (Suh et al., 1998). In Section 3 a description is given of the supporting hardware and software components that are needed to operate the ciliary array chip as a general-purpose manipulation tool. Section 4 provides results on the manipulation array that was used to move a silicon die. Finally, a summary of these results is provided in Section 5.
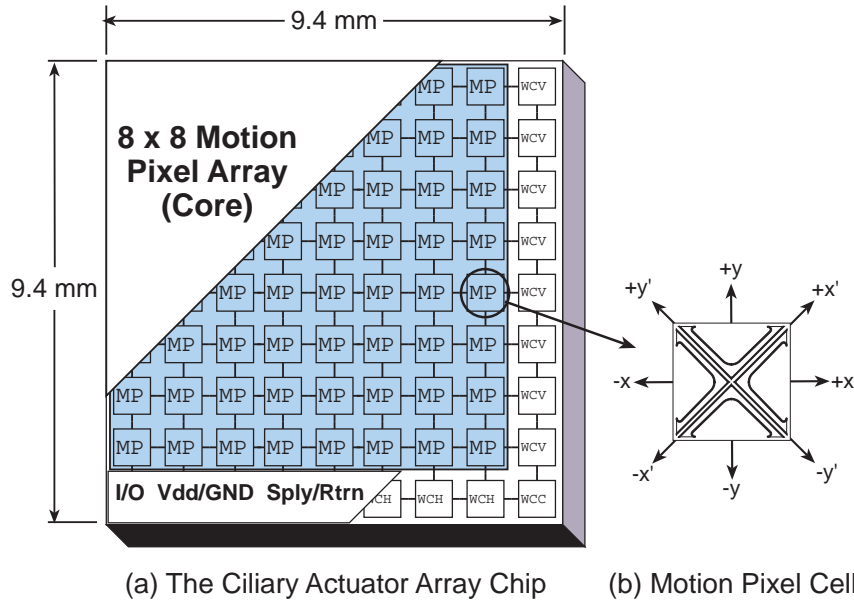

(a) The Ciliary Actuator Array Chip   (b) Motion Pixel Cell

Figure 1 The general architecture of the CMOS ciliary array is illustrated at left. Surrounding the 8×8 motion pixel (MP) cells are various circuits for input and output (I/O) of data, clocking, and power. The peripheral circuits contain a shift register chain which allows for both serial and parallel methods of loading data in the core. Each motion pixel cell (illustrated at right) has four triangle-shaped ciliary actuators.

2   SYSTEM ARCHITECTURE

2.1   CHIP ARCHITECTURE

The general architecture of the CMOS integrated ciliary array chip is shown in Figure 1a. The device is composed of two basic sections: the

array core and the periphery surrounding the array core on two sides. The array core consists of 256 ciliary actuators each with their associated logic and driver circuitry. The actuators are grouped into 64 1mm × 1mm cells (Figure 1b) and are arranged as an 8 × 8 array. Along the periphery of the core is a shift register chain, a mode select circuit, and row and column data loading circuits. The shift register chain consists of 16 cells, each of which has a shift register and a serial-parallel/row loader. These circuits provide the option of loading data into the individual cilia in a parallel or serial manner. The periphery also contains the voltage and ground bond pads for the logic circuits (Vdd/Gnd) and the power supply and return bond pads for the ciliary actuators. There are also eight sets of *Supply* and *Return* pads located in the horizontal wiring cells (one set per motion pixel column) to provide for a separate power supply voltage for the actuators (potentially above the logic supply).
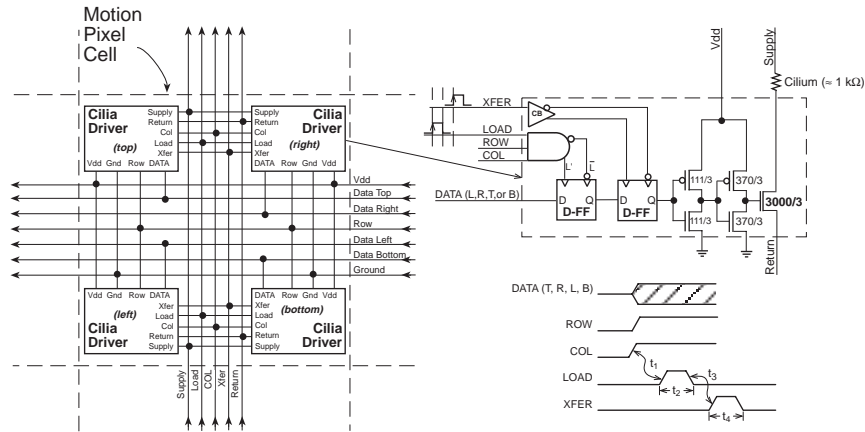

Figure 2 Block diagram of a motion pixel cell is illustrated at left. The cilia driver circuit is detailed in the upper right side of the figure. The driver consists of logic circuits, two series connected D-flip flops and a current driver. The timing necessary to run this circuit is shown in the lower right: $t_1 = Data$, *Row*, and *Col* setup time; $t_2 = Load$ pulse width; $t_3 = Load$ and *Xfer* clock dead time; $t_4 = Xfer$ pulse width.

2.2   MOTION PIXEL CELLS

The four ciliary actuators in each motion pixel are arranged orthogonally in a common-tip configuration. Each cilium has a driver circuit consisting of logic circuits and current drivers (Figure 2). In addition, the motion pixel cell has globally routed power and data interconnect lines that run parallel to its vertical and horizontal axes. Two series connected D-flip-flops (or phase registers) provide a buffering scheme so

that one register can be updated while the other register is controlling the actuator state. This arrangement enables simultaneous updating of all cilia. A register transfer signal enables the second register to change its state, thus transferring new data to the buffers and the MOSFET current driver.
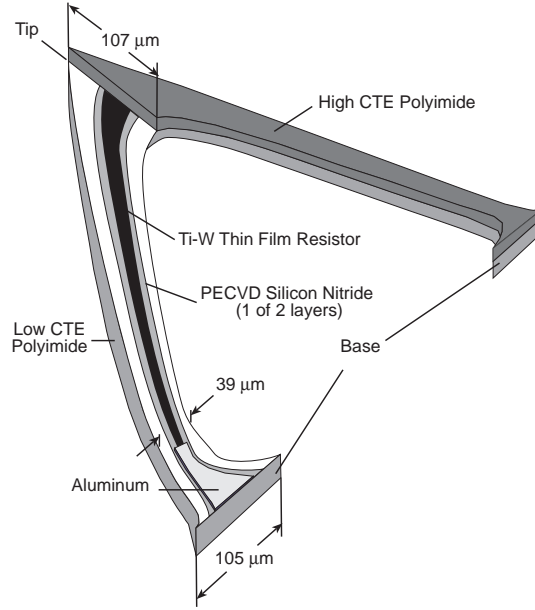

Figure 3 Illustration of the polyimide-bimorph thermal ciliary microactuator. In plan view (see Figure 1b), the actuator has the shape of two sides of an isosceles triangle. The base of the actuator is attached to the substrate at two locations. In this illustration, half of the upper polyimide and PECVD silicon nitride layers are shown removed to reveal the middle layers.

The ciliary actuator is a triangle-shaped structure fabricated using surface micromachining methods. The actuator is a multilayered structure made up of polyimide, silicon nitride, aluminum, and Ti-W films. Figure 3 is an illustration of the actuator with the upper polyimide and silicon nitride layers removed showing the relative placement of the other layers. The width of the cilium varies along its length: at the tip the beam is 107μm wide and gradually tapers to a width of 39μm near the base; at the base the actuator again widens to 105μm. The Ti-W heater resistor ($\approx 1000\Omega$) gradually widens from 10μm near the base to 28μm at the tip. The resistor is widest at the tip area to limit power dissipation and to lessen current crowding effects (Shibata et al., 1989) where the path of the resistor turns through $90°$.

Material	Typical Thickness μm	Young's Modulus GPa	Poisson's Ratio	CTE ppm/°C	Process Temp. °C	References
PIQ-3200	3.2-4.5	8.6	0.33	50	240	(Numata et al., 1988; Hitachi Chemical Co. Ltd., 1996)
PIQ-L200	3.2-4.5	2.95	0.33	2	240	(Numata et al., 1988; Hitachi Chemical Co. Ltd., 1996)
PECVD Silicon Nitride	0.12-0.14	183	0.25	1.5	300	(Stoffel et al., 1996; Hickernell et al., 1990)
50:50 Ti:W	0.09-0.1	340	0.2	4	25-40	(Glebovsky et al., 1995; Hartsough, 1979; Gere and Timoshenko, 1997)
Al	0.8-1.1	70	0.33	23.6	25-40	(Peterson, 1982; Gere and Timoshenko, 1997)

Table 1 Properties of the materials used in the fabrication of the ciliary actuator array.

Two important factors in the design of this actuator are the lifting capacity and the tip deflections. Through FEM simulations with the SO-LIDIS modeling tool (ISE Integrated Systems Engineering AG, Zurich, Switzerland, (Funk, 1995)), the lifting capacity of each actuator in a 1mm^2 motion pixel was estimated to be $\approx 80\mu\text{N}$ which is more than seven times the specific weight of a silicon die ($\approx 11\mu\text{N}/\text{mm}^2$). Further-more, the vertical displacement at the tip was computed to be $\approx 100\mu\text{m}$. These figures are comparable to another ciliary actuator described in (Suh et al., 1996; Suh et al., 1997) which clearly demonstrated the abil-ity to move a variety of small parts. The materials data (Table 1) used in the FEM simulations was obtained from various literature sources (Pe-terson, 1982; Numata et al., 1988; Hitachi Chemical Co. Ltd., 1996; Gle-bovsky et al., 1995; Hartsough, 1979; Stoffel et al., 1996; Hickernell et al., 1990; Gere and Timoshenko, 1997). Prior to simulation of the ciliary ac-tuator, the values were verified by running simulations of 2D models of

trimorph cantilever test structures (e.g., PIQ-3200/Al/PIQ-L200) fabricated alongside the ciliary array. The simulations of the test structure's vertical deflections were within 10% of those observed from SEM micrographs.

2.3   INPUT/OUTPUT CELLS

The peripheral cells contain voltage and ground pads and circuits that perform vital input and output (I/O) functions: row and column selection, serial data input/output pads, and cilia selection. The most important function performed by these peripheral cells is serial row and column selection which is accomplished by the 16-cell shift register chain that is routed around two edges of the array core.

Within each unit of the chain is a shift register cell and the serial/parallel row/column load circuit which allows the array to operate in either a serial or parallel loading mode. The serial mode is selected when the global control line *S/PSelect* is held at logic HIGH, while a LOW puts the chip into the parallel loading mode. Monitoring of the rows and columns that have been activated can be done when the array is in serial mode since the output of the shift register circuit drives a buffer that in turn drives the bond pads as an output. In parallel mode the pad buffers are put into a high impedance state, and the bond pads for each row or column directly drive the row or column buffers. Additionally, if the shift register cell output is disabled, the serial inputs have no effect on the row or column states.

3   EXPERIMENTAL SETUP

3.1   HARDWARE

A custom designed printed circuit board (PCB) was made to package the ciliary array chip and to provide the interface between the chip and the controlling personal computer (PC) system (see Figure 4). A CCD camera attached to a long working distance microscope enabled the user to observe the array. The output of the camera was viewed on a television monitor and recorded on a VHS tape recording system. The PC system was used to provide the user interface in addition to sending command data to the array.

The circuit board was designed to accommodate up to four ciliary array chips. A square hole in the center of the board was made so that a copper heat sink could be fastened to it. If necessary, heat can be actively drawn away by attaching a Peltier cooling device to the bottom of the heat sink. The ciliary chip was first bonded to the copper heat sink
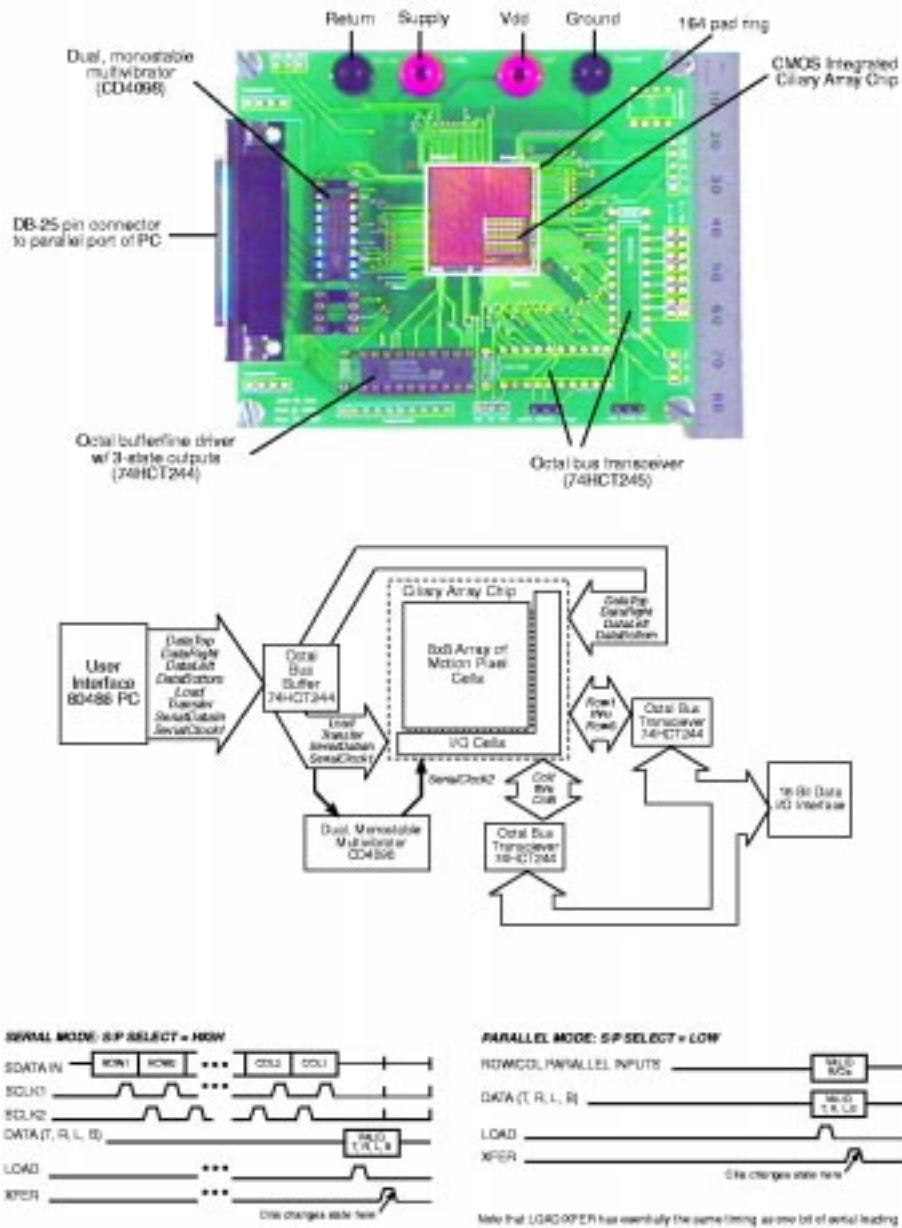
Figure 4 Overview of the general purpose micropositioning system. The CMOS ciliary array chip is packaged in a custom circuit board designed to operate up to 4 chips shown at the top figure, with a centimeter scale rule along its right edge. The block diagram in the middle of the figure shows the relation of the various components and connectors to the ciliary array chip. The timing diagram at the bottom shows how the array can be operated in either serial or parallel mode.

using a high-temperature curable die attach. Once attached, gold wire bonds were made between the chip and PC board using a ball bonder.

The assembly includes two ports for receiving command data: a DB-25 connector that receives data from a standard PC parallel port and a 2×8 pin header array which can be used to send data directly to each column and row. The 8-bit signal from the PC is routed to an octal bus buffer (74HCT244). The second shift register clock (*SClk2*) is generated on the board by the dual, monostable multivibrator (CD40948) and associated resistors/capacitors. The logic states of the shift registers can be monitored using an octal-bus transceiver (74HCT245) to receive data from the ciliary array. Alternatively, the bus transceiver can be used to directly load the rows and columns. (This requires twenty-two data inputs compared to the 8 input needed for operating the chip in serial mode). The timing required to update the array in either serial or parallel mode is shown in Figure 4.

3.2   SOFTWARE

Except for the voltage input settings, the ciliary array chip was completely under software control. Diagnostic software was first used to verify that each motion pixel could be individually controlled. The major function of the software was to regulate the gait sequences or to alter the way the actuators induced translation. It also allowed the array to be subdivided into smaller fields that are needed for doing vector field manipulations. Having the chip under software control enabled an unprecedented level of flexibility in operating a MEMS ciliary actuator array. A variety of low and high-level software functions have been programmed for both linear translation and squeeze field based manipulations (Böhringer et al., 1997a).

Control software was written in PASCAL and was implemented on a 80486-based PC. Signals were transferred by using the parallel port of the PC. The port's 8 databits consisted of the *DataTop*, *DataRight*, *DataLeft*, and *DataBottom* bits for activating the appropriate actuator, the *Load* and *Xfer* bits for writing the actuator state and activating the actuators, the *SData* (serial data) bit for writing addressing information into the shift register, and the *SClk1* bit.

Low level and benchmark functions.   A number of functions were used for testing of the basic functionality of the ciliary chip hardware.

Write one byte: This function allowed writing arbitrary user-specified test patterns without the need for function or word generators. The data can be typed in as binary or hexadecimal number.

Write byte sequence: A sequence of control signals was written at a user-specified frequency. These sequences usually consisted of a data signal for the actuator flip-flops or for the address register, followed by triggering of the *SClk1* bit.

Move one actuator: This function allowed a user to specify the address of an actuator. The software then generated a sequence of signals to (a) rewrite the data in the address register, (b) rewrite the data in the motion pixel, and (c) activate the motion pixel.

Scan all pixels: All actuators in the ciliary array were triggered in sequence at a user-specified frequency. This allowed easy visual inspection of malfunctioning cilia.

Speed test: A sequence of bytes was continuously written to the parallel port at a high frequency. This allowed determining the maximum switching speed of the CMOS circuitry.

High level functions. An actuator moved only if the data bit in its corresponding phase register was changed. Therefore, the actuators required a continuous flow of control signals. In general, these signal sequences consisted of address data, motion pixel data, and clock signals, which all depended on the intended array vector field. The software wrote a specific sequence of signals to the parallel port in real time.

Software for the higher level functions allowed the user to manipulate an object in a preprogrammed or in an interactive manner. Several useful control strategies were preprogrammed and could be chosen from a menu including linear translations for moving a part in the up, right, left, or down direction and vector fields for orienting a part along a vertical or horizontal squeeze line. For each of these strategies, a sequence of control signals was repeatedly written to the parallel port and can consist of many hundreds of individual byte signals.

Motion in arbitrary directions can be induced by alternating gaits that interleave gaits of different principal directions. For example, a translation at $25°$ from the x-axis requires motion in the y-direction and x-direction at a ratio of $\tan 25° \approx 1 : 2$. The control software determines the exact alternation for any translation angle analogously to the Bresenham line scan algorithm (Foley et al., 1996), resulting in different fields that are interleaved in time. This leads to the development of an interactive mode in which a user could, through keyboard commands, move an object at any speed and along any vector.

4   EXPERIMENTAL RESULTS

4.1   VERIFICATION OF CMOS WITH ARRAYED CILIARY ACTUATORS

All five test modules worked as expected, and the power required to achieve full deflection ranged from 35mW to 38 mW (input voltage range: 6.0V to 6.3V; input current range: 5.5mA to 6.4mA). Two ciliary array chips were used to check the functionality of the shift register chain by setting the *S/PSelect* pad at logic HIGH, connecting the *SClk1* and *SDataIn* pads to a digital word generator (HP-8006A), and monitoring the *SDataOut* pad. On both devices a data transfer rate of 25kHz was achieved, which was higher than necessary to run the manipulation tasks (described below).
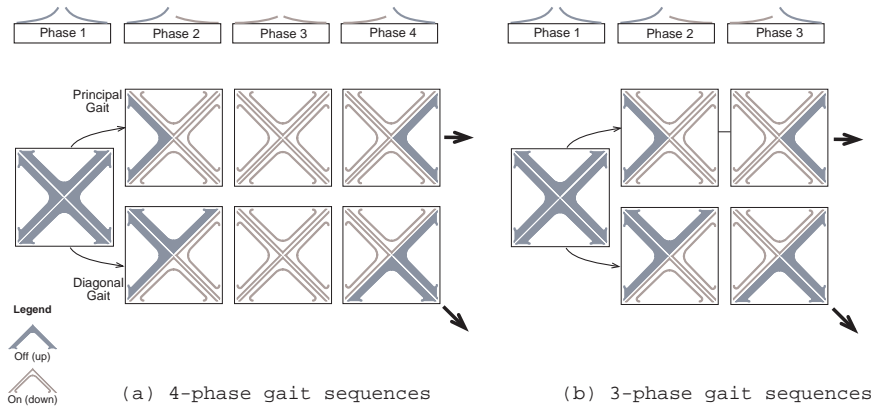

Figure 5 Illustration of different gaits: (a) 4-phase gaits. (b) A new 3-phase gait that omits one of the phases in the 4-phase gait. Standard gaits are shown on the top, virtual (diagonal) gaits on the bottom.

4.2   SIMPLE TRANSLATION EXPERIMENTS

Linear translation with principal gaits. Several sample parts were used in this experiment, however, the best results were obtained with a 3mm × 3mm × 0.1mm silicon die (from wafers supplied by Virginia Semiconductor, Inc., Fredericksburg, VA) of mass 1.7mg. The heaviest object moved was a 3mm × 3mm × 0.5mm silicon die (8.6mg). Video images of this demonstration are shown in Figure 6. The original FEM simulations indicated that the actual lifting capacity was $\approx 80\mu$N; however, these experiments indicate that the lifting capacity is less than estimated. To
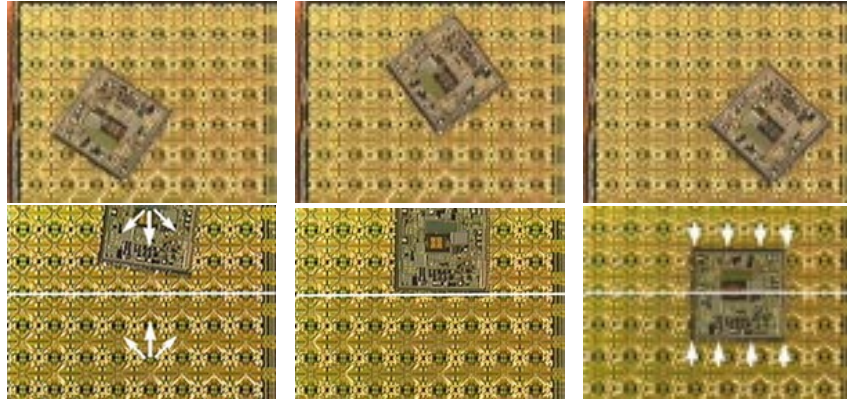
Figure 6   The top three images are frames from a video taken during arbitrary linear translation tests with 4-phase standard gaits.   These photos show that along with translation there is slight rotation that is not intended.
The bottom three images are from a video taken during a squeeze field manipulation test. Two diagonal gaits are used to produce a net perpendicular motion to the horizontal squeeze line (see left video image).The middle-bottom frame shows the part about to make contact with the opposing linear field. Right-bottom frame shows the part in rotational and translational equilibrium about the squeezeline.

move the Si die, each actuator received about 35mW of power. Since at the motion pixel level the principal gait has a 75 percent duty cycle, the total average power consumed by the entire array per gait was 6.7W.

Diagonal translation with virtual gaits.   The secondary method of moving an object was using a four-phase gait along the array's diagonals (e.g., Top-Right or Bottom-Left) and applying the appropriate gait pattern (see Figure 5). Since two actuators were commanded to act synchronously, diagonal gaits done in this way are also called virtual gaits because two actuators are working together as one. In this experiment, the actuators again received about 35mW of power, and the total average power consumed by the entire array (per gait) was 5.0W. This pattern uses less power than the principal gait due to the fact that its duty cycle for actuator hold-down is 50 percent.

It was observed that the motion induced by the virtual gaits was of a higher quality (smoother and faster) than the standard gait. Since using the action of two cilia to move an object effectively doubles the lifting capacity, the quality of induced motion is higher than the standard four-phase gait.
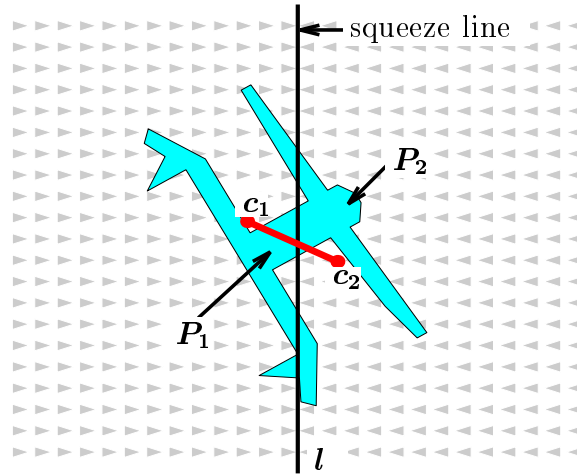
Figure 7 Equilibrium condition: To balance force and moment acting on part P in a unit squeeze field, the two areas P_1 and P_2 must be equal (i.e., l must bisect the part), and the line connecting the centers of area c_1 and c_2 must be perpendicular to the squeeze line l. Figure reprinted from (Böhringer et al., 1999b).
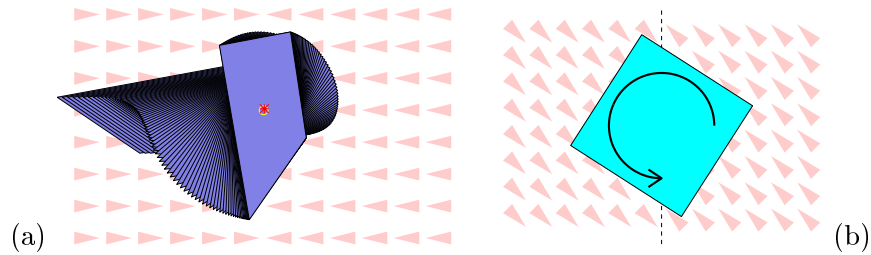

Figure 8 (a) Simulation of the alignment task with a unit squeeze field. Simulation techniques as well as geometric analysis were implemented to demonstrate how the manipulation of small parts can be automatically planned and controlled.
(b) Unstable square-shaped part in a skewed squeeze field ($\epsilon = -1$). The square with center on the squeeze line will rotate indefinitely. Moreover, it has *no* stable equilibrium in this field.

4.3   VECTOR FIELD EXPERIMENTS

Control for Squeeze Fields.   Consider the following family of control strategies called *squeeze fields* (Böhringer et al., 1994; Böhringer et al., 1997a) and a manipulation planning algorithm for parts-orientation (see Figures 7 and 8a).

Definition 1 (Böhringer et al., 1997a) *Given a straight line l, a squeeze field f is a two-dimensional force vector field in which, at each point, a unit force points perpendicularly towards l (on l the force is zero).*

The line l is called the *squeeze line*, because l lies in the center of the squeeze field.

Assuming quasi-static motion, an object will translate and rotate to an equilibrium configuration, as characterized in Figure 7. To predict the equilibria, a uniform force distribution over the surface of P is assumed, which is an appropriate model for a flat part that is in contact with a large number of elastic actuators.

Definition 2 *A part P is in* translational equilibrium *if the forces acting on P are balanced. P is in* orientational equilibrium *if the moments acting on P are balanced.* Total equilibrium *is simultaneous translational and orientational equilibrium.*

Claim 3 *Every squeeze field f (see Definition 1) has potential, of the form $U(\mathbf{z}) = \int_{\alpha} f \cdot ds$, where α is an arbitrary path to $\mathbf{z}$ from a fixed reference point. If $d_{\mathbf{z}}$ denotes the perpendicular distance of $\mathbf{z}$ from the squeeze line, then $U(d_{\mathbf{z}}) = |d_{\mathbf{z}}|$.*

Claim 4 (Böhringer et al., 1997a) *Let P be a connected polygonal part with finite contact area and n vertices. Then in any squeeze field, P has $E = O(rn^2)$ orientation equilibria, where r is the maximum number of edges that a bisector of P can cross. If P is convex, then the number of equilibria is $O(n)$.*

Equilibria can be calculated numerically using the method in Figure 7: Given an arbitrary part at a fixed orientation, it is translated until its left and right sections have equal size. If the respective centers of gravity lie on a line perpendicular to the squeeze line, then the part is in equilibrium. For polygonal parts there exist analytical methods to compute the equilibria exactly. See (Böhringer et al., 1997a) for a detailed algorithm and a derivation of the $O(rn^2)$ bound.

Claim 5 (Böhringer et al., 1997a) *Let P be a polygon whose interior is connected. There exists a sensorless alignment strategy consisting of a sequence of squeeze fields that uniquely orients P up to symmetries.*[1]

4.3.1 Task: Orienting and Aligning Parts. If a part is placed in a squeeze field, it will translate and rotate until a stable equilibrium
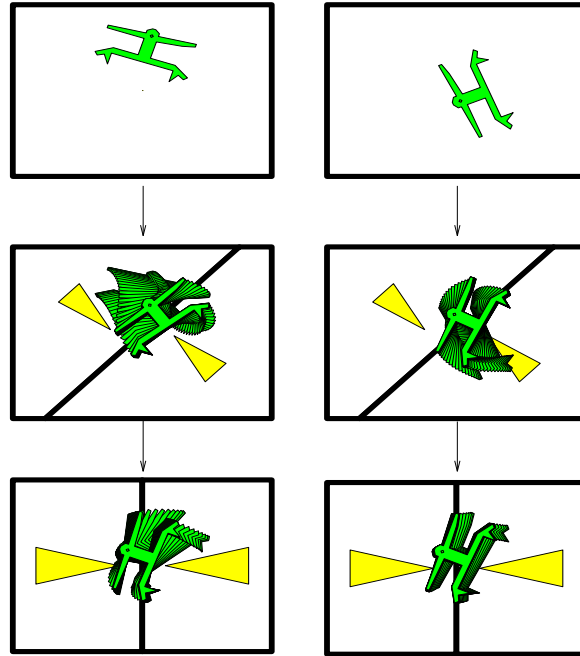
Figure 9 Sensorless parts orienting using force vector fields: the part reaches unique orientation from an arbitrary initial pose after two consecutive squeezes. There exist such orientating strategies for all polygonal parts. Figure reprinted from (Böhringer et al., 1999b).

is reached (Claim 4). Parts may exhibit several equilibria, hence after one squeeze the part orientation may be ambiguous. This ambiguity can be removed with the strategies of Claim 5: by executing a sequence of squeezes at particular angles, the part is uniquely oriented (see Figure 9). Note that this task, as well as all those described below, are sensorless, i.e., they do not require sensor feedback.

Squeeze fields. To carry out this task the ciliary array was subdivided into two fields each consisting of either a 4×8 (vertical squeeze line) or 8×4 (horizontal squeeze line) array of motion pixel cells. Squeeze fields with both principle and diagonal direction gaits were implemented. The diagonal gaits had equal proportions $\pm 45°$ to produce a net translation towards the squeeze line.

Various silicon chips were placed near the edge of the ciliary array at the beginning of the experiment. The squeeze field pushed the chips towards the center. Both centering and orienting was observed in good

agreement with the predictions from theory and simulation. For square parts two kinds of equilibria were observed: (1) square diagonal coinciding with the squeeze line, and (2) central axis coinciding with the squeeze line. Equilibrium (1) is predicted from the theory of (continuous) force fields. In ideal continuous fields, (2) is an unstable equilibrium. However, (Luntz et al., 1998) showed that for actuator arrays with discrete contacts, (2) may become a stable equilibrium. These experimental observations indicate that effects from the discrete character of the ciliary array are significant.
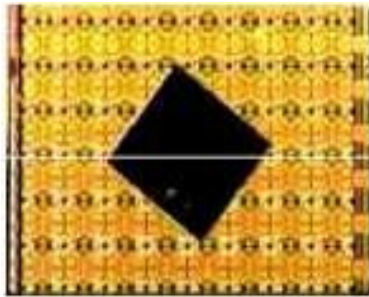

Figure 10   A 3mm × 3mm × 0.1mm square die after reaching stable equilibrium in a squeeze field. The squeeze line is drawn in white.

Images from the video taken during these experiments are shown in Figure 10, which shows a square part after reaching a stable equilibrium in category (1), and also in Figure 6, which shows a part as it reaches and equilbrium in category (2). In our experiments, the equilibria in category (1) were achieved more frequently.

4.3.2   Task: Centering.   Squeeze fields achieve a centering effect only along one axis. Radial fields can center a part in two dimensions. These fields are discussed in this section.

Radial fields.

Definition 6 *A radial field R is a two-dimensional force vector field such that $R(\mathbf{z}) = -\mathbf{z}/|\mathbf{z}|$ if $\mathbf{z} \neq 0$, and $R(\mathbf{0}) = \mathbf{0}$.*

Claim 7 *A radial field has a potential, $U(\mathbf{z}) = |\mathbf{z}|$.*

Claim 8 (Böhringer et al., 1997a) *Given a polygonal part P in a radial field R, there exists a unique pivot point v of P such that P is in equilibrium if and only if v coincides with the center of the radial field. v is typically not the center of mass of P.*

Claim 9 (Böhringer et al., 1997a) *Let P be a polygonal part with n vertices, and let r be the maximum number of edges that a bisector of P can cross. There are at most $E = O(rn)$ stable equilibria in a field of the form $R + \delta S$ if S is a squeeze field, and δ is sufficiently small and positive.*

Proofs of the previous claims, and a numerical algorithm to compute the pivot point is given in (Böhringer et al., 1997a). Note that Claim 9 results in strategies for unique part posing in $O(E^2) = O(r^2 n^2)$ time.

Radial fields can be used to center a part. The previous generation four-quadrant cilia device (Böhringer et al., 1997b) implemented an approximation of an ideal radial field similar to the field in Figure 9. Note that this approximate radial field has a potential whose shape is in the form of an upside-down square pyramid.

With the current fully addressable design a single cilia array suffices to generate such a radial field. Parts centering was demonstrated in recent experiments with (among others) a 3mm × 3mm × 0.1mm chip.

4.3.3   Task: Rotation.   Squeeze fields and radial fields cause stable equilibria in parts placed into them. The previous sections exploited this effect to perform open-loop positioning and orienting strategies, and to predict the final pose of a part. However, an equally useful task might be the continuous translation and rotation of a part, for example for inspection of micro-parts under a microscope. This is the focus of the next paragraphs.

Four-quadrant circular fields.   A field that causes rotation was described by (Fujita, 1993) and (Liu and Will, 1995). The four quadrants generate forces in East, South, West, and North directions, creating a discretized vortex. The cilia array was programmed to implement this field. Note that this field also has a centering effect which was observed in the experiment.

Skewed squeeze fields.   A *skewed field* f_S is a vector field given by $f_S(x, y) = -\text{sign}(x)(1, \epsilon)$, where $\epsilon \in \mathbb{R} \backslash \{0\}$. No skewed squeeze field has a potential (Böhringer et al., 1997a). In a skewed squeeze field, it is easy to find a circular path along which the work integral is non-zero (e.g., along a circle with center on the squeeze line). A skewed field induces *no* stable equilibrium on a disk-shaped part (for all $\epsilon \neq 0$, see (Böhringer et al., 1997a)). Translational equilibrium is only possible if the center of the disk coincides with the squeeze line. In this position the disk experiences a non-zero moment if $\epsilon \neq 0$. Finally, a diagonally skewed field ($\epsilon = \pm 1$) induces *no* stable equilibrium on a square-shaped part.[2]

According to the dynamic model above, certain parts will rotate indefinitely in skewed squeeze fields (Figure 8b). Note that even though the cilia device has more degrees of freedom, two areas of constant force are sufficient to implement a skewed field, resulting in a very simple task-level rotation strategy. In particular, the rotation algorithm resulting from the application of skew-symmetric squeeze fields is considerably simpler than previous rotation algorithms (for example, the vortices suggested by (Fujita, 1993) or by (Liu and Will, 1995) as described above). While vortices require at least four areas of the array to be pushing in different directions. skewed fields perform the same task with only two regions of constant force.

Diagonal gaits are a particularly simple and effective means to implement skewed fields. The array is subdivided into two rectangular areas with opposing diagonal gaits. For example, if the left half pushes in SE direction, and the right half pushes in NW direction, we obtain a skewed field with $\epsilon = -1$, which causes a counterclockwise rotation (see again Figure 8b).

Skewed squeeze fields were implemented both with the previous and with the new array design. While the former suffered from the fact that the rotation occurred essentially on top of the gap between two separate cilia chips, the new chip was able to implement a full skewed squeeze field on a single array. This resulted in a much smoother rotation motion as well as in an increase in speed by about a factor 10. 360° rotation was possible in less than 1 minute.

4.3.4   Task: Unique Positioning with Universal Fields.   Recently it was shown that there exist families of force fields that generate *unique* equilibria for all non-symmetric parts (Böhringer et al., 1999a).

Definition 10 *A combined radial gravity field is defined as $f_\delta(x, y) = R(x, y) + \delta G$ where R is a radial field as defined above, $G = (0, -1)$ is a unit "gravity" field in the $-y$ direction, and $0 \leq \delta \leq 1$.*

Claim 11 (Böhringer et al., 1999a) *Let P be an arbitrary non-symmetric polygonal part. There exists a δ such that P has a unique equilibrium in f_δ.*

This result may give rise to a new generation of parts feeding and positioning devices that do not require any hardware adjustments when the part design is changed, nor do they require sensor feedback or programming.

Tilted radial fields.   A "universal field" was implemented for the first time with the cilia array. The radial component was generated with a

unit radial field R as described above. To add the gravity component δG, the array was tilted by a small angle ϕ. A nonsymmetric quadrilateral part was used (part sides approximately 1.1mm, 5.3mm, 2.5mm, and 4.3mm, thickness 0.1mm) for these experiments. Initially, for $\delta = 0$ no unique equilibrium was observed. Preliminary experiments showed that by a tilt angle of a few degrees, the part always settled in the same equilibrium.
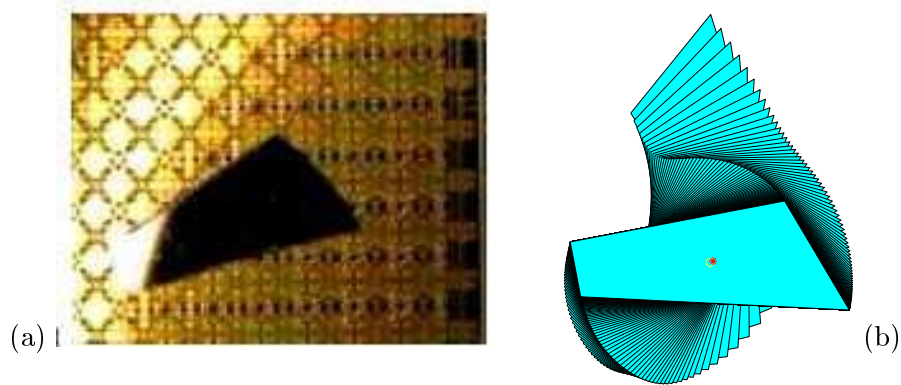

(a)   (b)

Figure 11 A "universal field" implemented with a cilia array. (a) In preliminary experiments, the quadrilateral silicon chip was placed on the array implementing a radial field. When the array was tilted to the right, the part consistently reached the same equilibrium from arbitrary initial configurations. (b) Simulation run of the quadrilateral part in the universal field $R + 0.5G$, which corresponds to a tilt angle of approximately $\phi = 30°$.

In Figure 11a the quadrilateral part has reached a stable equilibrium on the tilted cilia array. Figure 11b shows the corresponding simulation with a field $R + 0.5G$. Reasons for the discrepancy between equilibrium orientations in simulation and experiment may include an inaccurate estimate of the δ factor, as well as variations in the performance of the individual actuators, and the relatively small number of discrete actuators in contact with the quadrilateral chip.

5   SUMMARY

The ciliary chip described herein is the first micromanipulation array fabricated directly on top of control circuits. This degree of integration enables each actuator to be separately addressable and turns the array into a reconfigurable micromanipulation device. The design of the previous ciliary array described in (Suh et al., 1996) limited it to performing linear translations. The current array was designed to perform vector field manipulations such as orienting, alignment, and centering in addi-

tion to arbitrary linear translations without having to tile chips together as was done with the previous arrays.

Realization of this ciliary array was carried out by surface micro-machining polyimide-based actuators on substrates with pre-fabricated CMOS circuits. Only a few chips needed to be packaged for the tests in this paper because the operational yield was excellent. Over all the chips tested, only a few motion pixels exhibited less than expected performance during operation. No problems due to thermal degradation such as loss of adhesion between layers was observed during testing.

Validation of this approach was achieved through the demonstration of the chip with individual motion pixels, simple uniform vector fields, or subdivided vector fields. Translation along arbitrary vectors and squeeze field centering and alignment were successfully demonstrated, as well as centering with a radial field. Preliminary experiments on a "universal parts feeder" were also performed successfully.

Acknowledgments

Notes

1. The proof is interesting: Claim 4 states that a squeeze field brings a polygon P into one of $E = O(rn^2)$ orientation equilibria. We define the *squeeze function* as this mapping from original orientation to equilibrium orientation. Hence, from Claim 4 it follows that the image of the squeeze function is a set of E discrete values. Given such a squeeze function, Goldberg has presented an algorithm for sensorless manipulation of polygons (Goldberg, 1993) that constructs an orienting strategy with $O(E)$ steps in $O(E^2)$ time. The output of this algorithm is a sequence of squeeze directions. When the corresponding squeeze fields are applied to the part P, the set of possible orientations is successively reduced until a unique orientation (up to symmetry) is reached. For details see (Böhringer et al., 1997a) and (Goldberg, 1993).

2. For a proof see (Böhringer et al., 1997a).

References

Ataka, M., Omodaka, A., and Fujita, H. (1993). A biomimetic micro motion system. In *Transducers — Digest Int. Conf. on Solid-State Sensors and Actuators*, pages 38–41, Pacifico, Yokohama, Japan.

Baltes, H. (1993). CMOS as sensors technology. *Sensors and Actuators A (Physical)*, A37-A38:51–56.

Baltes, H. (1996). Future of IC microtransducers. *Sensors and Actuators A (Physical)*, A56(1–2):179–192.

Berlin, A. A. and Gabriel, K. J. (1997). Distributed MEMS: New challenges for computation. *IEEE Computer Science and Engineering*, pages 17–29.

Bobbio, S. M., Kellam, M. D., Dudley, B. W., Goodwin-Johnasson, S., Jones, S. K., J. D. Jacobson, M. T., and DuBois, T. D. (1991). Integrated force arrays. In *Proc. IEEE Workshop on Micro Electro Mechanical Systems (MEMS)*, pages 74–79, Ft. Lauderdale, FL.

Böhringer, K.-F., Donald, B. R., Kavraki, L., and Lamiraux, F. (1999a). Part orientation with one or two stable equilibria using programmable vector fields. *IEEE Transactions on Robotics and Automation*. Submitted for review.

Böhringer, K.-F., Donald, B. R., and MacDonald, N. C. (1996). Single-crystal silicon actuator arrays for micro manipulation tasks. In *Proc. IEEE Workshop on Micro Electro Mechanical Systems (MEMS)*, pages 7–12, San Diego, CA.

Böhringer, K.-F., Donald, B. R., and MacDonald, N. C. (1997a). Upper and lower bounds for programmable vector fields with applications to MEMS and vibratory plate parts feeders. In Laumond, J.-P. and Overmars, M., editors, *Algorithms for Robotic Motion and Manipulation*, pages 255–276. A. K. Peters, Ltd, Wellesley, MA 02181.

Böhringer, K.-F., Donald, B. R., and MacDonald, N. C. (1999b). Programmable vector fields for distributed manipulation, with applica-

tions to MEMS actuator arrays and vibratory parts feeders. *Int. Journal of Robotics Research*.

Böhringer, K.-F., Donald, B. R., MacDonald, N. C., Kovacs, G. T. A., and Suh, J. W. (1997b). Computational methods for design and control of MEMS micromanipulator arrays. *IEEE Computer Science and Engineering*, pages 17–29.

Böhringer, K.-F., Donald, B. R., Mihailovich, R., and MacDonald, N. C. (1994). A theory of manipulation and control for microfabricated actuator arrays. In *Proc. IEEE Workshop on Micro Electro Mechanical Systems (MEMS)*, pages 102–107, Oiso, Japan.

Busch-Vishniac, I. J. (1991). Micro-automating semiconductor fabrication. *IEEE Circuits & Devices*, 7(4):32–37.

Chen, L. Y., Santos, E. J. P., and MacDonald, N. C. (1991). An isolation technology for joined tungsten MEMS. In *Proc. IEEE Workshop on Micro Electro Mechanical Systems (MEMS)*, pages 189–194, Ft. Lauderdale, FL.

Foley, J. D., Van Dam, A., Feiner, and Hughes (1996). *Computer Graphics: Principles and Practice*. Addison Wesley, Reading, MA, 2nd edition.

French, P. J. (1996). Development of surface micromachining techniques compatible with on-chip electronics. *Journal of Micromechanics and Microengineering*, 6(2):197–211.

Fujita, H. (1993). Group work of microactuators. In *International Advanced Robot Program Workshop on Micromachine Technologies and Systems*, pages 24–31, Tokyo, Japan.

Fujita, H. and Gabriel, K. J. (1991). New opportunities for micro actuators. In *Transducers — Digest Int. Conf. on Solid-State Sensors and Actuators*, pages 14–20, San Fransisco, CA.

Funk, J. (1995). *Modeling and Simulation of IMEMS*. PhD thesis, ETH Zürich, Zürich, Switzerland.

Furuhata, T., Hirano, T., and Fujita, H. (1991). Array-driven ultrasonic microactuators. In *Transducers — Digest Int. Conf. on Solid-State Sensors and Actuators*, pages 1056–1059, Montreux, France.

Gere, J. M. and Timoshenko, S. P. (1997). *Mechanics of Materials*. PWS Publishing Co., Boston, MA, 4 edition.

Glebovsky, V. G., Yaschak, V. Y., Baranov, V. V., and Sackovich, E. L. (1995). Properties of titanium-tungsten thin films obtained by magnetron sputtering of composite cast targets. *Thin Solid Films*, 257(1):1–6.

Goldberg, K. Y. (1993). Orienting polygonal parts without sensing. *Algorithmica*, 10(2/3/4):201–225.

Hartsough, L. D. (1979). Resistivity of bias-sputtered ti-w films. *Thin Solid Films*, 64(1):17–23.

Hickernell, T. S., Fliegel, F. M., and Hickernell, F. S. (1990). The elastic properties of thin-film silicon nitride. In *IEEE Ultrasonics Symp. Proc.*, volume 1, pages 445–448.

Hitachi Chemical Co. Ltd. (1996). Hitachi chemical literature and data sheets for their PIQ and PIX polyimides. Available from HD MicroSystems (an enterprise of Hitachi Chemical and DuPont Electronics.

Hornbeck, L. J. (1995). Digital light processing and MEMS: Timely convergence for a bright future. In *Proc. SPIE*, volume 2642, page 2. (abstract only); full text available from Texas Instruments, Dallas, TX.

Howe, R. T. (1995). Polysilicon integrated microsystems: Technologies and applications. In *Transducers — Digest Int. Conf. on Solid-State Sensors and Actuators*, volume 1, pages 43–46, Stockholm, Sweden.

Klaassen, E. H., Reay, R. J., and Kovacs, G. T. A. (1996). Diode-based thermal R.M.S. converter with on-chip circuitry fabricated using CMOS technology. *Sensors and Actuators A (Physical)*, A52(1–3):33–40.

Konishi, S. and Fujita, H. (1994). A conveyance system using air flow based on the concept of distributed micro motion systems. *Journal of Microelectromechanical Systems*, 3(2):54–58.

Liu, C., Tsai, T., Tai, Y.-C., Liu, W., Will, P., and Ho, C.-M. (1995). A micromachined permalloy magnetic actuator array for micro robotics assembly systems. In *Transducers — Digest Int. Conf. on Solid-State Sensors and Actuators*, volume 1, pages 328–331, Stockholm, Sweden.

Liu, W. and Will, P. (1995). Parts manipulation on an intelligent motion surface. In *IEEE/RSJ Int. Workshop on Intelligent Robots & Systems (IROS)*, volume 3, pages 399–404, Pittsburgh, PA.

Lund, J. L. and Wise, K. D. (1994). Chip-level encapsulation of implantable CMOS microelectrode arrays. In *Proc. Solid State Sensor and Actuator Workshop*, pages 29–32, Hilton Head, SC.

Luntz, J. E., Messner, W., and Choset, H. (1998). Velocity field design for parcel positioning on the virtual vehicle, a discrete distributed actuator array. In Agarwal, P. K., Kavraki, L., and Mason, M., editors, *Robotics: The Algorithmic Perspective*. A. K. Peters, Ltd, Wellesley, MA.

Minami, M., Kawamura, S., and Esahi, M. (1993). Distributed electrostatic micro actuator (dema). In *Transducers — Digest Int. Conf. on Solid-State Sensors and Actuators*, pages 2–3, Yokohama, Japan. Late news contribution.

Mita, Y., Konishi, S., and Fujita, H. (1997). Two dimensional micro conveyance system with through holes for electrical and fluidic interconnection. In *Transducers — Digest Int. Conf. on Solid-State Sensors and Actuators*, volume 1, pages 37–40, Chicago, IL.

Moser, D., Lenggenhager, R., and Baltes, H. (1991). Silicon gas flow sensors using industrial CMOS and bipolar IC technology. *Sensors and Actuators A (Physical)*, A25(4):577–581.

Nakazawa, H., Watanabe, Y., and Morita, O. (1997). The two-dimensional micro conveyor: Principles and fabrication process of the actuator. In *Transducers — Digest Int. Conf. on Solid-State Sensors and Actuators*, volume 1, pages 33–36, Chicago, IL.

Nasby, D., Hetherington, D. L., Sniegowski, J. J., Apblett, C. A., Smith, J. H., Montague, S., Barron, C. C., Eaton, W., and MacWhorter, P. J. (1996). Application of chemical-mechanical polishing to planarization of surface-micromachined device. In *Proc. Solid State Sensor and Actuator Workshop*, pages 48–53, Hilton Head, SC.

Numata, S., Miwa, T., Misawa, U. Y., Makino, D., Imaizumi, J., and Kinjo, N. (1988). Low thermal expansion polyimides and their applications. In *Proc. Mat. Res. Soc. Symp.*, volume 18, pages 113–124.

Offenberg, M., Lärmer, F., Elsner, B., Münzel, H., and Riethmüller, W. (1995). Novel process for a monolithic integrateda ccelerometer. In *Transducers — Digest Int. Conf. on Solid-State Sensors and Actuators*, volume 1, pages 589–592, Stockholm, Sweden.

Peterson, K. E. (1982). Silicon as a mechanical material. *Proc. IEEE*, 70(5):420–457. classic paper on early MEMS.

Pister, K. S. J., Fearing, R., and Howe, R. (1990). A planar air levitated electrostatic actuator system. In *Proc. IEEE Workshop on Micro Electro Mechanical Systems (MEMS)*, pages 67–71, Napa Valley, California.

Shibata, S., Kanamori, T., and Tsuruoka, T. (1989). Development of heating resistor for versatile thermal print heads. *IEEE Trans. on Components, Hybrids, and Mfg. Tech.*, 12(3):358–364.

Spangler, C. and Kemp, C. J. (1996). A smart automotive accelerometer with on-chip airbag deployment circuits. In *Proc. Solid State Sensor and Actuator Workshop*, pages 221–214, Hilton Head, SC.

Stoffel, A., Kovacs, A., Kronast, W., and Mueller, B. (1996). LPCVD and PECVD for micromechanical applications. *Journal of Micromechanics and Microengineering*, 6(1):1–13.

Suh, J. W., Darling, R. B., Böhringer, K.-F., Baltes, H., Donald, B. R., and Kovacs, G. T. A. (1998). CMOS integrated organic ciliary array for general-purpose micromanipulation tool for small objects. *Journal of Microelectromechanical Systems*. Submitted for review.

Suh, J. W., Glander, S. F., Darling, R. B., Storment, C. W., and Kovacs, G. T. A. (1996). Combined organic thermal and electrostatic omnidirectional ciliary microactuator array for object positioning and inspection. In *Proc. Solid State Sensor and Actuator Workshop*, pages 168–173, Hilton Head, SC.

Suh, J. W., Glander, S. F., Darling, R. B., Storment, C. W., and Kovacs, G. T. A. (1997). Organic thermal and electrostatic ciliary microactuator array for object manipulation. *Sensors and Actuators A (Physical)*, 58:51–60.

Takeshima, N. and Fujita, H. (1991). Polyimide bimorph actuators for a ciliary motion system. In *ASME WAM Symposium on Micromechanical Sensors, Actuators, and Systems*, volume DSC-32, pages 203–209.